General Method for Determining the Masses of Semi-Invisibly Decaying Particles at Hadron Colliders

Konstantin T. Matchev and Myeonghun Park

Phys. Rev. Lett. **107**, 061801 — Published 1 August 2011

DOI: 10.1103/PhysRevLett.107.061801

A general method for determining the masses of semi-invisibly decaying particles at hadron colliders

Konstantin T. Matchev and Myeonghun Park
Physics Department, University of Florida, Gainesville, FL 32611, USA

We present a general solution to the long standing problem of determining the masses of pair-produced, semi-invisibly decaying particles at hadron colliders. We define two new transverse kinematic variables, $M_{CT_\perp}$ and $M_{CT_\parallel}$, which are suitable one-dimensional projections of the contransverse mass M_{CT}. We derive analytical formulas for the boundaries of the kinematically allowed regions in the $(M_{CT_\perp}, M_{CT_\parallel})$ and $(M_{CT_\perp}, M_{CT})$ parameter planes, and introduce suitable variables $D_{CT_\parallel}$ and D_{CT} to measure the distance to those boundaries on an event per event basis. We show that the masses can be reliably extracted from the endpoint measurements of $M_{CT_\perp}^{max}$ and D_{CT}^{min} (or $D_{CT_\parallel}^{min}$). We illustrate our method with dilepton $t\bar{t}$ events at the LHC.

PACS numbers: 14.80.Ly,12.60.Jv,11.80.Cr

The ongoing run of the Large Hadron Collider (LHC) at CERN will finally provide the first glimpse of physics at the TeV scale. Complementary and independent arguments from particle physics *and* astrophysics suggest that the best place to look for new physics is a channel with missing transverse energy $\not{E}_T$, caused by unseen new particles contributing to the dark matter of the Universe.

Unfortunately, missing energy signatures pose a tremendous challenge at the LHC, where in each event, the partonic center-of-mass energy $\sqrt{\hat{s}}$ and longitudinal momentum p_z of the initial state are unknown. To make matters worse, the lifetime of the dark matter particle is typically protected by a new parity symmetry, which guarantees that the missing particles come in pairs, thus proliferating the number of unknown parameters describing the final state event kinematics.

The generic topology of a "new physics" $\not{E}_T$ event is sketched in Fig. 1. Consider the *inclusive* production of an identical pair of new "parent" particles P. Each parent P decays semi-invisibly to a set V_i $(i = 1, 2)$ of standard model (SM) particles, which are visible in the detector, and a dark matter particle C (from now on referred to as the "child") which escapes detection. In general, the parent pair is accompanied by a number of additional "upstream" objects U (typically jets) with total transverse momentum $\vec{U}_T$. They may originate from various sources such as initial state radiation or decays of even heavier particles. Given this general setup, the goal is to determine *independently* the mass M_p of the parent and the mass M_c of the child in terms of U, V_1 and V_2.

In the past, several approaches to this problem have been proposed, but each has its own limitations. For example, the classic method of invariant mass endpoints [1] only applies when the visible SM particles in V_i arise from a sufficiently long decay chain. Attempts at direct reconstruction [2] of the children momenta are again limited to long decay chains only. In this letter, we shall consider the extreme, most challenging example where each visible set V_i consists of a *single* SM particle of fixed mass m_i. A perfect testing ground for this scenario is provided by dilepton $t\bar{t}$ events (already observed at the LHC [3]) and we shall use that example in our numerical illustrations below. The role of the parent P (child C) will be played by the SM W-boson (SM neutrino), each V_i is a SM lepton (e or μ), while U is composed of the two b-jets from the top quark decays, plus any additional QCD jets from initial state radiation

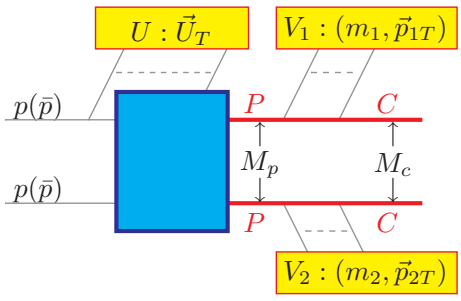

FIG. 1: The generic event topology under consideration. All particles visible in the detector are clustered into three groups: upstream objects U with total transverse momentum $\vec{U}_T$, and two composite visible particles V_i $(i = 1, 2)$, each with invariant mass m_i and total transverse momentum $\vec{p}_{iT}$.

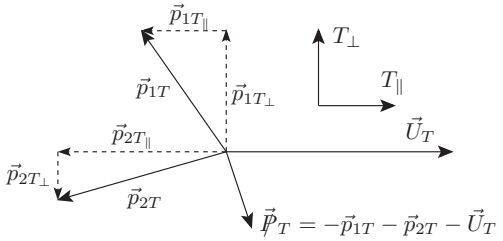

FIG. 2: Decomposition of the observed transverse momentum vectors from Fig. 1 in the transverse plane.

(ISR).

For such extremely short decay chains, the only viable alternative at the moment is provided by the methods based on the M_{T2} variable [4]. There, at least in principle, the individual masses M_p and M_c can be determined by observing a "kink" feature in the M_{T2} endpoint as a function of a hypothesized trial mass M_c for C [5], or by exploring the U_T dependence of the M_{T2} endpoint [6]. Compared to those M_{T2} approaches, our method here has two advantages. First, it is simpler – it uses only the observed objects U, V_1 and V_2 in the event and makes no reference to the missing particle kinematics (or mass). Second, it is more precise, since it utilizes the whole kinematic boundary of the relevant *two-dimensional* distribution and not just the kinematic endpoint of its *one-dimensional* projection. We proceed in three easy steps.

Step I. Orthogonal decomposition of the observed transverse momenta with respect to the $\vec{U}_T$ direction. The Tevatron and LHC collaborations currently use fixed axes coordinate systems to describe their data. Instead, we propose to rotate the coordinate system from one event to another, so that the transverse axes are always aligned with the direction $T_\parallel$ selected by the measured upstream transverse momentum vector $\vec{U}_T$ and the direction $T_\perp$ orthogonal to it (see Fig. 2). The visible transverse momentum vectors from Fig. 1 are then decomposed as

$$\vec{p}_{iT_\parallel} \equiv \frac{1}{U_T^2}\left(\vec{p}_{iT}\cdot\vec{U}_T\right)\vec{U}_T, \tag{1}$$

$$\vec{p}_{iT_\perp} \equiv \vec{p}_{iT} - \vec{p}_{iT_\parallel} = \frac{1}{U_T^2}\vec{U}_T \times \left(\vec{p}_{iT}\times\vec{U}_T\right). \tag{2}$$

Step II. Constructing the transverse and longitudinal contransverse masses $M_{CT_\perp}$ and $M_{CT_\parallel}$. Our starting point is the original contransverse mass variable [7] which is invariant under longitudinal Lorentz boosts and rotations with respect to the beam axis:

$$M_{CT} = \sqrt{m_1^2 + m_2^2 + 2\left(e_{1T}e_{2T} + \vec{p}_{1T}\cdot\vec{p}_{2T}\right)}, \tag{3}$$

where e_{iT} is the "transverse energy" of V_i

$$e_{iT} = \sqrt{m_i^2 + |\vec{p}_{iT}|^2}. \tag{4}$$

For events with $U_T = 0$, M_{CT} has an upper endpoint which is insensitive to the unknown $\sqrt{\hat{s}}$, providing one relation among M_p and M_c [7, 8]

$$M_{CT}^{max}(U_T = 0) = \sqrt{m_1^2 + m_2^2 + 2m_1m_2\cosh\left(\zeta_1 + \zeta_2\right)}, \tag{5}$$

where

$$\sinh\zeta_i \equiv \frac{\lambda^{\frac{1}{2}}(M_p^2, M_c^2, m_i^2)}{2M_p m_i}, \tag{6}$$

$$\lambda(x,y,z) \equiv x^2 + y^2 + z^2 - 2xy - 2xz - 2yz\,. \tag{7}$$

Unfortunately, the $U_T = 0$ limit is not particularly interesting at hadron colliders (especially for inclusive studies), since a significant amount of upstream U_T is typically generated by ISR (and other) jets. One possible fix is to use all events, but modify the definition (3) to approximately compensate for the transverse $\vec{U}_T$ boost [8]. One then recovers

a distribution whose endpoint is still given by (5). Alternatively, one could stick to the original M_{CT} variable, and simply account for the U_T dependence of its endpoint as

$$M_{CT}^{max}(U_T) = \sqrt{m_1^2 + m_2^2 + 2m_1 m_2 \cosh(2\eta + \zeta_1 + \zeta_2)} \tag{8}$$

where ζ_i were already defined in (6), and

$$\sinh\eta \equiv \frac{U_T}{2M_p}, \quad \cosh\eta \equiv \sqrt{1 + \frac{U_T^2}{4M_p^2}}\,. \tag{9}$$

Our approach here is to utilize eqs. (1,2) and construct one-dimensional analogues of the M_{CT} variable

$$M_{CT_\perp} \equiv \sqrt{m_1^2 + m_2^2 + 2\,(e_{1T_\perp} e_{2T_\perp} + \vec{p}_{1T_\perp}\cdot\vec{p}_{2T_\perp})}, \tag{10}$$

$$M_{CT_\parallel} \equiv \sqrt{m_1^2 + m_2^2 + 2\left(e_{1T_\parallel} e_{2T_\parallel} + \vec{p}_{1T_\parallel}\cdot\vec{p}_{2T_\parallel}\right)}, \tag{11}$$

where the corresponding "transverse energies" are

$$e_{iT_\perp} \equiv \sqrt{m_i^2 + |\vec{p}_{iT_\perp}|^2}, \quad e_{iT_\parallel} \equiv \sqrt{m_i^2 + |\vec{p}_{iT_\parallel}|^2}. \tag{12}$$

The benefit of the decomposition (10,11) is that one gets "two for the price of one", i.e. two independent and complementary variables instead of the single variable (3).

The variable $M_{CT_\perp}$ in particular is very useful for our purposes. To illustrate the basic idea, it is sufficient to consider the most common case, where V_i is approximately massless ($m_i = 0$), as the leptons in our $t\bar{t}$ example. A crucial property of $M_{CT_\perp}$ is that its endpoint is independent of U_T:

$$M_{CT_\perp}^{max} = \frac{M_p^2 - M_c^2}{M_p}, \quad \forall\ U_T. \tag{13}$$

In fact the whole $M_{CT_\perp}$ distribution is insensitive to U_T:

$$\frac{\mathrm{d}N}{\mathrm{d}M_{CT_\perp}} = N_{0_\perp}\,\delta(M_{CT_\perp}) + (N_{tot} - N_{0_\perp})\,\frac{\mathrm{d}\bar{N}}{\mathrm{d}M_{CT_\perp}}, \tag{14}$$

where $N_{0_\perp}$ is the number of events in the zero bin $M_{CT_\perp} = 0$. Using phase space kinematics, we find that the shape of the remaining (unit-normalized) zero-bin-subtracted distribution is simply given by

$$\frac{\mathrm{d}\bar{N}}{\mathrm{d}\hat{M}_{CT_\perp}} \equiv -4\,\hat{M}_{CT_\perp}\ln\hat{M}_{CT_\perp} \tag{15}$$

in terms of the unit-normalized $M_{CT_\perp}$ variable

$$\hat{M}_{CT_\perp} \equiv \frac{M_{CT_\perp}}{M_{CT_\perp}^{max}}. \tag{16}$$

Fig. 3a shows the $M_{CT_\perp}$ distribution of the two leptons in our $t\bar{t}$ sample, for 10 fb^{-1} of LHC data at 7 TeV. Events were generated with PYTHIA [9] and processed with the PGS detector simulator [10]. We apply standard background rejection cuts as follows [3]: we require two isolated, opposite sign leptons with $p_{iT} > 20$ GeV, $m_{\ell^+\ell^-} > 12$ GeV, and passing a Z-veto $|m_{\ell^+\ell^-} - M_Z| > 15$ GeV; at least two central jets with $p_T > 30$ GeV and $|\eta| < 2.4$; and a $\not\!\!E_T$ cut of $\not\!\!E_T > 30$ GeV ($\not\!\!E_T > 20$ GeV) for events with same flavor (opposite flavor) leptons. We also demand at least two b-tagged jets, assuming a flat b-tagging efficiency of 60%. With those cuts, the SM background from other processes is negligible [3].

Fig. 3a demonstrates that the $M_{CT_\perp}$ endpoint can be measured quite well. Since the theoretically predicted shape (15) is distorted by the cuts, we use a linear slope with Gaussian smearing, and fit for the endpoint and the resolution parameter. We find $M_{CT_\perp}^{max} = 80.9$ GeV (compare to the true value $M_{CT_\perp}^{max} = 80.4$ GeV), which gives one constraint (13) among M_p and M_c. At this point, a second, independent constraint can in principle be obtained from an analogous

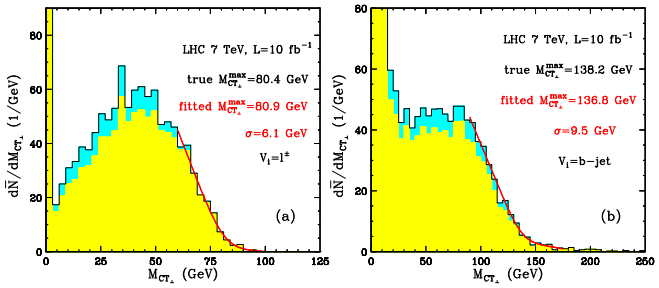

FIG. 3: $M_{CT_\perp}$ distributions after cuts, for $t\bar{t}$ dilepton events. The visible particles V_i are selected to be the two leptons in (a) and the two b-jets in (b). The yellow (lower) portion is our signal, while the blue (upper) portion shows $t\bar{t}$ combinatorial background with isolated leptons arising from τ or b decays.

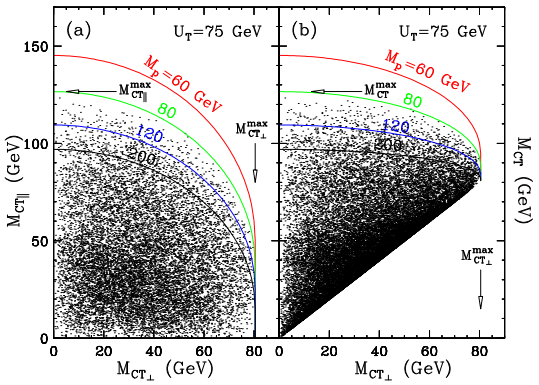

FIG. 4: Scatter plots of (a) $M_{CT_\perp}$ versus $M_{CT_\parallel}$ and (b) $M_{CT_\perp}$ versus M_{CT}, for a fixed representative value $U_T = 75$ GeV. The solid lines show the corresponding boundaries defined in (20) and (23), for the correct value of $M_{CT_\perp}^{max}$ and several different values of M_p as shown.

measurement of the M_{CT}^{max} endpoint (8) at a fixed value of U_T (resulting in loss in statistics), after which the two masses can be found from

$$M_p = \frac{U_T\, M_{CT}^{max}(U_T)\, M_{CT_\perp}^{max}}{(M_{CT}^{max}(U_T))^2 - (M_{CT_\perp}^{max})^2}, \tag{17}$$

$$M_c = \sqrt{M_p\,(M_p - M_{CT_\perp}^{max})}. \tag{18}$$

However, the orthogonal decomposition (10,11) offers another approach, which we pursue in the last step.

Step III. Fitting to kinematic boundary lines. It is known that two-dimensional correlation plots reveal a lot more information than one-dimensional projected histograms [11]. To this end, consider the scatter plot of $M_{CT_\perp}$ vs $M_{CT_\parallel}$ in Fig. 4a, where for illustration we used 10,000 events at the parton level. For a given value of $M_{CT_\perp}$, the allowed values of $M_{CT_\parallel}$ are bounded by

$$M_{CT_\parallel}^{(lo)}(M_{CT_\perp}) \le M_{CT_\parallel} \le M_{CT_\parallel}^{(hi)}(M_{CT_\perp}), \tag{19}$$

where $M_{CT_\parallel}^{(lo)}(M_{CT_\perp}) = 0$ and

$$M_{CT_\parallel}^{(hi)}(M_{CT_\perp}) = M_{CT_\perp}^{max}\left(\sqrt{1-\hat{M}_{CT_\perp}^2}\cosh\eta + \sinh\eta\right). \tag{20}$$

Fig. 4a reveals that the endpoint $M_{CT_\parallel}^{max}$ of the one-dimensional $M_{CT_\parallel}$ distribution is obtained at $M_{CT_\perp} = 0$

$$\begin{aligned} M_{CT_\parallel}^{max} &= M_{CT_\parallel}^{(hi)}(0) = M_{CT_\perp}^{max}(\cosh\eta + \sinh\eta) \\ &= \frac{1}{2}\left(1 - \frac{M_c^2}{M_p^2}\right)\left(\sqrt{4M_p^2 + U_T^2} + U_T\right). \end{aligned} \tag{21}$$

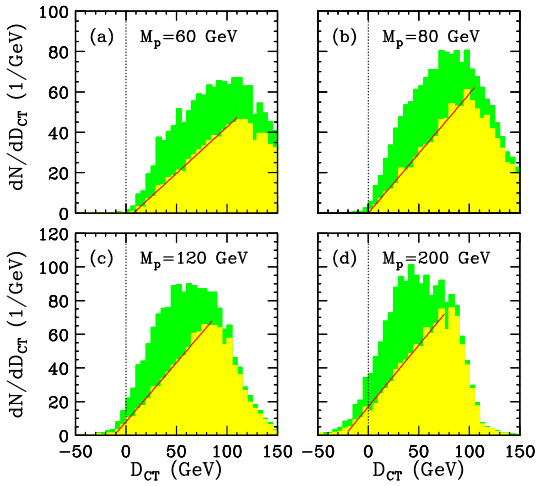

FIG. 5: D_{CT} distributions for four different values of M_p (and M_c given from (18)). The yellow (light shaded) histograms use only events in the zero bin $M_{CT_\perp} = 0$. The red solid lines show linear binned maximum likelihood fits.

Notice that events in the zero bins $M_{CT_\perp} = 0$ and $M_{CT_\parallel} = 0$ fall on one of the axes and cannot be distinguished on the plot.

Now consider the scatter plot of $M_{CT_\perp}$ vs M_{CT} shown in Fig. 4b. M_{CT} is similarly bounded by

$$M_{CT}^{(lo)}(M_{CT_\perp}) \le M_{CT} \le M_{CT}^{(hi)}(M_{CT_\perp}), \tag{22}$$

where this time $M_{CT}^{(lo)}(M_{CT_\perp}) = M_{CT_\perp}$ and

$$M_{CT}^{(hi)}(M_{CT_\perp}) = M_{CT_\perp}^{max}\left(\cosh\eta + \sqrt{1-\hat{M}_{CT_\perp}^2}\,\sinh\eta\right). \tag{23}$$

We see that the endpoint M_{CT}^{max} of the one-dimensional M_{CT} distribution is also obtained for $M_{CT_\perp} = 0$:

$$M_{CT}^{max} = M_{CT}^{(hi)}(0) = M_{CT_\perp}^{max}(\cosh\eta + \sinh\eta) = M_{CT_\parallel}^{max}. \tag{24}$$

Fig. 4 reveals a conceptual problem with one-dimensional projections. While *all* points in the vicinity of the boundary lines (20) and (23) are sensitive to the masses, the $M_{CT_\perp}^{max}$ endpoint is extracted mostly from events with $M_{CT_\perp} \sim M_{CT_\perp}^{max}$, while the $M_{CT_\parallel}^{max}$ and M_{CT}^{max} endpoints are extracted mostly from the events with $M_{CT_\perp} \sim 0$. The events near the boundary, but with *intermediate* values of $M_{CT_\perp}$, will not enter efficiently either one of these endpoint determinations.

So how can one do better, given the knowledge of the boundary line (23)? In the spirit of [12], we define the signed distance to the corresponding boundary, e.g.

$$D_{CT}(M_p, M_c) \equiv M_{CT}^{(hi)}(M_{CT_\perp}, U_T, M_p, M_c) - M_{CT}$$

and similarly for $D_{CT_\parallel}$. The key property of this variable is that for the correct values of M_p and M_c, its lower endpoint D_{CT}^{min} is exactly zero (see Fig. 5b):

$$D_{CT}^{min}(M_p, M_c) = 0, \tag{25}$$

and the boundary line (23) provides a perfectly snug fit to the scatter plot — notice the green boundary line marked "80" in Fig. 4b. While in general eq. (25) represents a two-dimensional fit to M_p and M_c, in practice one can already use the $M_{CT_\perp}^{max}$ measurement from Fig. 3a to reduce the problem to a single degree of freedom, e.g. the parent mass M_p, as presented in Figs. 4 and 5. The correct choice of parent mass $M_p = 80$ GeV provides a perfect envelope in Fig. 4b, resulting in $D_{CT}^{min} = 0$ in Fig. 5b. If, on the other hand, M_p is too low, a gap develops between the outlying points in the scatter plot of Fig. 4b and their expected boundary (23), which results in $D_{CT}^{min} > 0$, as illustrated in Fig. 5a. Conversely, if M_p is too high, some of the outlying points from the scatter plot fall outside the boundary (23) and have $D_{CT} < 0$, leading to $D_{CT}^{min} < 0$, as seen in Figs. 5c and 5d. The resulting fit for D_{CT}^{min} as a function of M_p

from our PGS data sample is shown in Fig. 6, suggesting that a W mass measurement at the level of a few percent might be viable.

The method can also be used to measure the top quark mass itself. To this end, all one needs to do is to select $V_i = b$ as the visible particles of Fig. 1. The resulting $M_{CT_\perp}$ distribution is shown in Fig. 3b. Fitting its endpoint as before, we obtain $136.78^{+2.97}_{-4.04}$ GeV (to be compared with the true value of 138.20 GeV). Since the b-jet has some non-negligible mass, we cannot use (13), but instead need to go back to (8) and set $\eta = 0$, since by construction the component of $\vec{U}_T$ along $T_\perp$ is zero. We obtain a measurement of the top mass as $173.83^{+2.45}_{-3.32}$ GeV, to be contrasted with the nominal value of 175 GeV used in our simulations.

Acknowledgments. This work is supported in part by a US Department of Energy grant DE-FG02-97ER41029.

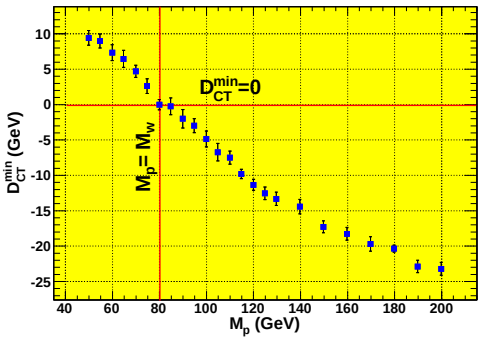

FIG. 6: Fitted values of D_{CT}^{min} as a function of M_p.

[1] I. Hinchliffe *et al.*, Phys. Rev. D **55**, 5520 (1997).
[2] K. Kawagoe, M. M. Nojiri and G. Polesello, Phys. Rev. D **71**, 035008 (2005); H. C. Cheng *et al.*, Phys. Rev. Lett. **100**, 252001 (2008).
[3] V. Khachatryan *et al.* [CMS Collaboration], arXiv:1010.5994 [hep-ex].
[4] C. G. Lester and D. J. Summers, Phys. Lett. B **463**, 99 (1999); A. Barr, C. Lester and P. Stephens, J. Phys. G **29**, 2343 (2003).
[5] A. J. Barr, B. Gripaios and C. G. Lester, JHEP **0802**, 014 (2008); M. Burns, K. Kong, K. T. Matchev and M. Park, JHEP **0903**, 143 (2009).
[6] K. T. Matchev, F. Moortgat, L. Pape and M. Park, Phys. Rev. D **82**, 077701 (2010); P. Konar, K. Kong, K. T. Matchev and M. Park, Phys. Rev. Lett. **105**, 051802 (2010).
[7] D. R. Tovey, JHEP **0804**, 034 (2008).
[8] G. Polesello and D. R. Tovey, JHEP **1003**, 030 (2010).
[9] T. Sjostrand, S. Mrenna and P. Skands, JHEP **0605**, 026 (2006).
[10] http://www.physics.ucdavis.edu/∼conway/research/software/pgs/pgs4-general.htm
[11] D. Costanzo and D. R. Tovey, JHEP **0904**, 084 (2009); M. Burns, K. T. Matchev and M. Park, JHEP **0905**, 094 (2009); K. T. Matchev, F. Moortgat, L. Pape and M. Park, JHEP **0908**, 104 (2009).
[12] I. W. Kim, Phys. Rev. Lett. **104**, 081601 (2010).